Available online at www.sciencedirect.com
ScienceDirect
Journal of Power Sources 162 (2006) 513–520
JOURNAL OF POWER SOURCES
www.elsevier.com/locate/jpowsour

Analysis of PEMFC freeze degradation at −20 °C after gas purging

Junbo Hou [a,b], Hongmei Yu [a,*], Shengsheng Zhang [a,c], Shucheng Sun [a], Hongwei Wang [a], Baolian Yi [a], Pingwen Ming [a]

[a] *Fuel Cell R & D Center, Dalian Institute of Chemical Physics, Chinese Academy of Sciences, 457 Zhongshan Road, Dalian 116023, PR China*
[b] *Graduate School of the Chinese Academy of Sciences, Beijing 100039, PR China*
[c] *School of Science, Beijing Jiaotong University, Beijing 100044, China*

Received 8 June 2006; received in revised form 30 June 2006; accepted 3 July 2006
Available online 9 August 2006

Abstract

Proton exchange membrane fuel cell (PEMFC) freeze degradation was investigated using 20 freeze/thaw cycles of two cells with gases purged immediately after operation. The cell purged by gas with an RH 58.0% at 25 °C was found to have no performance loss after the 20 freeze/thaw cycles. From the cell resistances and the electrochemical impedance spectra (EIS), the electrolyte conductivity and interfacial charge transfer resistance were unchanged. The electrochemical active surface area (ECSA) from the cyclic voltammetry (CV) measurements indicated that the amount of water in the catalyst layer of the cell was reduced to an extent that the damage in the freeze/thaw cycles was avoided. Another cell was purged by RH 64.9% gas in the first cycle, and then was purged with RH 45.0% gas in 19 freeze/thaw cycles. Although the cell easily became flooded at high current densities after the first cycle, no further performance loss was found. The pore size distribution data from mercury intrusion porosimetry measurements suggested that the gas diffusion layer was changed by the first freeze cycles. The micrographs (SEM) further proved no membrane electrode assembly (MEA) delamination. These results shed some light on the relationship of the water amount in the cell to subzero temperature exposure.

Keywords: Subzero storage; Degradation; Relative humidity; Proton exchange membrane fuel cell (PEMFC)

1. Introduction

Worldwide attention has been paid to proton exchange membrane fuel cells (PEMFCs), owing to their potential importance in the hydrogen economy. As a promising candidate for the substitution of the internal combustion engine, PEMFCs will experience different environment conditions including a cold winter. Although much effort has been devoted to the PEMFCs development on materials such as effective catalysts [1,2] and membranes [3,4], operation conditions [5] and cell behavior [6,7], only a few papers focus on the behavior of fuel cells at subzero temperatures. For PEMFC commercialization, this should be investigated.

When a PEMFC operates, water is produced at the cathode side due to the oxygen reduction reaction. Once the cell shuts down and is kept at subzero temperature, generally the water in the cell will freeze. Water freezing may have a negative impact on the fuel cell materials and components. Widely used proton exchange membranes, i.e., Nafion®, are proton conductors only when water is present. McDonald et al. [8] found that if the water amount in Nafion® 112 membrane was about 1.6–3.4 wt.%, there was no catastrophic damage after 386 freeze/thaw (−40 to 80 °C) cycles. For Nafion® 115, in either a dry state with water amounts less than 3 wt.% or a wet state, the membrane conductivity was almost constant (0.0323–0.0319 S cm^{-1}) after four freeze/thaw (−10 to 30 °C) cycles [9]. The state of water in the membrane is a key issue. From differential scanning calorimetry measurement (DSC) [10], there were three kinds of water in the proton conductive polymer including nonfreezing water, freezable loosely bound water and free water. Morihiro et al. [11] reported that even at −20 °C, although the free water froze, the nonfreezing water remained and it was movable in the Nafion®. However, the effect of water freezing on the membrane characteristics still needs further work. The volume change caused

* Corresponding author. Tel.: +86 411 84379051; fax: +86 411 84379185.
E-mail address: hmyu@dicp.ac.cn (H. Yu).

0378-7753/$ – see front matter © 2006 Elsevier B.V. All rights reserved.
doi:10.1016/j.jpowsour.2006.07.010

by the water/ice phase transition definitely destroys the catalyst layer (CL) and the gas diffusion layer (GDL) structure. By N_2 adsorption and BET analysis, the number of the pores (pore size more than 25 nm) increase while the number of smaller pores decrease. As a result, the specific surface area of catalyst layer decreases [9]. The gas and water passages in the diffusion layer are also influenced by water freezing. Oszcipok et al. [12] tested the hydrophobicity of the channel pattern on the GDL surface. They found that it became slightly more hydrophilic. However, the pore size in the catalyst layer and diffusion layer ranges from nanometers to micrometers, and water in the pores should have different freezing behavior [13,14]. In addition, performance degradation caused by water freezing was found [9]. After four freeze/thaw cycles (−10 to 80 °C), a degradation rate of 2.8% at 0.6 V was observed as well as a reduction of electrochemical active surface area.

To prevent PEMFCs material performance degradation, water removal methods, i.e., dry N_2 gas purging, were applied. But during the purging process the membrane dehydrates, which may impede successful start-up, especially following freezing. Since not all water molecules in the micropores freeze down to −20 °C, it is possible to purge the cell to a certain RH. In this study, we use reactant gases with different RHs to purge the cells immediately after the cell operation. Cell degradation with different RHs has been investigated using 20 freeze/thaw cycles.

2. Experimental

2.1. Gas diffusion electrodes and MEA fabrication

A 20 wt.% E-TEK Pt/C (Vulcan XC-72) catalyst, Toray carbon paper, Nafion® solution and PTFE suspension were used to fabricate the electrodes. The Pt loading of the gas diffusion electrodes (GDEs) was 0.8 mg cm^{-2} and the dry Nafion® content was about 1.0 mg cm^{-2} for both anode and cathode. More details are reported by our research group [15]. The N212 membrane was sandwiched between the two electrodes. The MEA sealed with O-rings had an effective area of 4 cm^2.

2.2. Fuel cell hardware and polarization curve measurements

The single cell consisted of an MEA, two graphite bipolar plates and two organic glass end plates. Graphite polar plates used as current collectors were machined with parallel flow channels. The other side of the graphite planar plate was machined with channels for the coolant. A silicon O-ring was used as a seal. The fuel cell test station consisted of temperature controllers, humidifiers, mass-flow controllers, pressure regulators and an impedance meter (KFM2030 Kikusui, Japan). The experimental data were recorded by Fuel Cell Load & Impedance software from Kikusui. The cell was operated at 0.2 MPa and 60 °C, while the reactant humidification temperatures were set at 5 °C and 10 °C above the cell temperature. The heating tape temperatures were 7 °C higher than the humidification temperatures to avoid water condensation. The cathode and anode outlet gas flows were controlled at a constant flow rate of 100 and 40 mL min^{-1}. Additional flows of 3.5 and 7 mL min^{-1} A^{-1} for the cathode and anode were provided depending on the current. The cell was firstly operated at 0.25 A cm^{-2} for 0.5 h, followed by conditioning at 0.5 A cm^{-2} for 0.5 h, at 1 A cm^{-2} for another 0.5 h and operating at 0.5 A cm^{-2} until the voltage became stable. Then, the polarization curve was recorded.

Three cells were used. MEA1 was purged with dry reactant gas after operation, but without freezing. MEA2 and MEA3 were frozen at −20 °C for 1.5 h after purging with different relative humidity gases. After the cell operation, the reactant gases were continually fed into the cell, and the flow rate was controlled from 800 to 100 mL min^{-1} because of the decreasing pressure drop between the gas inlet and outlet. The whole purging process lasted about 5 min. MEA2 was purged by RH 58.0% at 25 °C reactant gas to RH 16.6% at 50 °C through all freeze/thaw cycles. For the first thermal cycle, MEA3 was purged by RH 64.9% at 25 °C reactant gas. From the 2nd to 20th freeze/thaw cycle, it was purged to RH 12.9% at 50 °C using RH 45.0% at 25 °C reactant gas. The values of the RH were obtained using a hygrometer (Vaisala HMT360, Finland). After the purging, the cell gas inlets and outlets were sealed, then, put into a climate-controlled chamber. To avoid other impacts, such as membrane dehydration, masking the cell performance and to accurately investigate the degradation caused by only water freezing, the cell was stabilized at 0.5 A cm^{-2} for 0.5 h with the gas flow rate mentioned before each polarization test.

Cell internal resistance, referred to as the high frequency resistance (HFR) was measured at 10 kHz. The measurement was performed by an impedance meter superimposing a 10 kHz sinusoidal signal with an amplitude of 165 mA (peak to peak) with the cell in the galvanostatic mode.

2.3. Catalyst active surface area measurements

An additional diagnostic test, cyclic voltammetry, was implemented to determine the electrochemical surface area (ECSA) of the cathode electrode available for hydrogen adsorption or desorption. A TDI3691 potentiostat (TianJing ZhongHuan, China) was used. The humidified hydrogen and ultrahigh purity nitrogen gas was fed to the anode and the cathode, with flow rates of 40 and 100 mL min^{-1}, respectively. The reference and counter electrode leads were connected to the anode while the working electrode lead was connected to the cathode. For the CV, three cycles were performed at a sweep rate of 50 mV s^{-1} and cell potential was scanned from −0.05 to 1.0 V.

2.4. Electrochemical impedance spectra (EIS)

In situ electrochemical impedance spectra were measured by a KFM2030 impedance meter. The perturbation amplitude for the sinusoidal signal was 165 mA (peak to peak) over a frequency range of 10 kHz to 0.1 Hz. For comparative experiments among the different freeze/thaw cycles, impedance measurements were performed after the polarization test. The cell was stabilized at 0.5 and 1 A cm^{-2} respectively for 3 min, before the perturbation was added to the cell.

2.5. SEM and mercury intrusion porosimetry measurements

The specimens for SEM were prepared by cutting the MEA with a surgical knife. The SEM measurements were performed on a Jeol (JSM-5600LV) scanning electronic microscope.

The porosity of the MEAs was measured by the mercury intrusion method with a PoremasterGT60 (Quantachrome). The pressure was from 1.38×10^3 to 4.13×10^7 Pa (0.2–6. 0×10^4 psi) and the mercury contact angle was 140°.

3. Results and discussion

3.1. Fuel cell performance after gas purging

Polarization curves and high frequency resistances of MEA2 and MEA3 are shown in Fig. 1. The "0" represents the initial performance characteristics, ECSA, and EIS. In Fig. 1a, no performance loss is observed over the entire current density range, even up to 1.5 A cm^{-2}. But in Fig. 1b, deviation in the diffusion region is found. The performance loss compared with the original is attributed to mass transport limitations, because in the first gas purging process, the relative humidity in the cell was higher than RH 16.6%. Water vapor in the cell condensed in the flow channels and in the GDL while the cell was cooled in the climate chamber. It is most likely that the volume expansion of water freezing slightly changes the GDL structure, and the loss of hydrophobicity in the GDL might be another reason [12]. This can be seen in Fig. 1b, with deviation only in the high current density region. From the second thermal cycle, the purging reactant gas relative humidity was controlled as RH 45.0%, and the relative humidity in the cell was RH 12.9%. No progressive performance loss in the mass transport limitation region was observed, but the GDL was easily flooded in the high current density region. A similar phenomenon was found in St-Pierre work [16]. They purged the cell at about 85 °C immediately after cell operation. As a result, progressive performance loss was observed due to mass transport. They suggested purging at about 20 °C was more effective. In our experiment, reactant gas with a certain relative humidity was continually fed after cell operation. Faster gas flow rate was achieved by a high pressure drop between the cell inlet and outlet. When the RH at the cell outlet came to the expected values, i.e., RH 16.6% at 50 °C, the purging was stopped. By this method, the water amount can be reduced effectively.

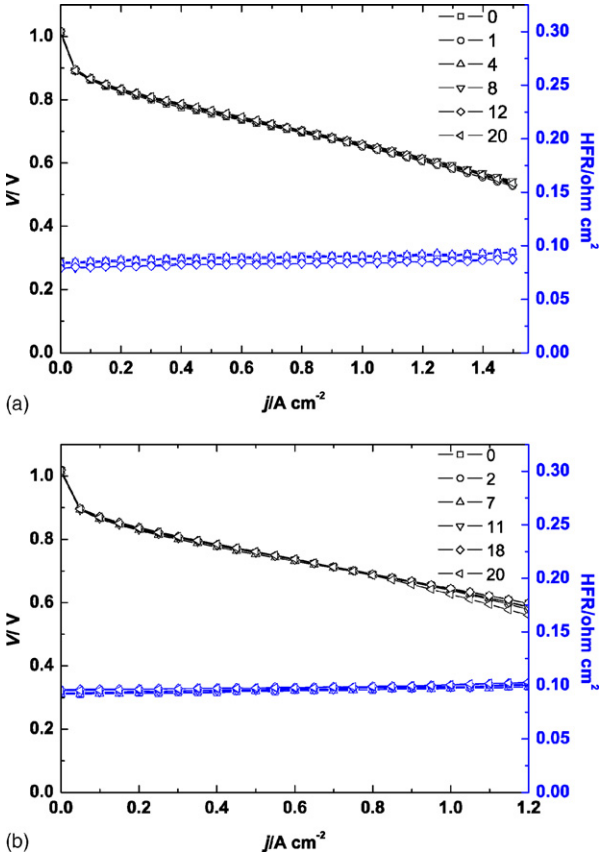

Fig. 1. *I–V* plots and high frequency resistances of MEAs before/after frozen: (a) MEA2; (b) MEA3.

The high frequency resistances of the cells are also shown in Fig. 1. Although the HFR at 10 kHz is slightly above the real axis in the Nyquist plot, it approximately equals the cell resistance. So the HFR can be assumed to be the sum of the material bulk resistance and the interfacial contact resistance. The cell resistance increases with the current density, but not insignificantly. This is due to the membrane on the anode side dehydrating at high current density. For the Nafion® 117 membrane, a 150% current density increase would result in a 144% decrease in maximum water content of the membrane at the anode side [17]. Consequently, there is a water gradient across the membrane. For MEA2, from 0 to 1.5 A cm^{-2}, the resistance increases from 83.97 to 94.18 mΩ cm^2, with an increase of 12.16%. After 20 freeze/thaw cycles, from 0 to 1.5 A cm^{-2}, the resistance became 81.27 mΩ cm^2 to 90.45 mΩ cm^2—an increase of 11.30%. The difference of the increase is very small. As a result, the properties of the membrane governing the back diffusion of water, such as the hydraulic permeability and water diffusivity, do not change significantly. Although the relative humidities of the purging gas and the cell after water removal are known, the amount of water in the membrane cannot be calculated accurately. The reason is the water in the membrane will drain out when the cell was cooled down to −20 °C. However, the residual water in the membrane cannot make catastrophic destroy. For MEA3, in the first freeze/thaw cycle, higher RH (RH 64.9%) reactant gas was used. The resistance increase from 0 to 1.2 A cm^{-2} becomes larger, from 6.59 to 11.10% after the first cycle. From the 2nd to the 20th thermal cycle, RH 45.0% reactant gas was used to purge the cell and a lower RH 12.9% in the cell after purging was achieved. The resistance increase is from 11.10 to 8.44% in the remaining 19 thermal cycles. The slight decrease implies the water freezing effect on the membrane characteristics is small. Some Refs. [18,19] reported that under high temperature and adverse humidification conditions, the hot pressed membrane could not be easily or fully rehydrated. We carried out another cell (MEA1) start-up and shutdown experiment without the freeze process. After the cell operation, the cell was purged by dry reactant gas for 5 min, and the RH in the cell was controlled to 3% at 50 °C. The case that the cell could not start up at

0.5 A cm^{-2} within 15 s was encountered for several times. The cell resistance increased to 0.8 Ω cm^2. After 20 start-up and shut-down cycles, the resistance at 1 A cm^{-2} increased from 104.48 to 114.34 mΩ cm^2.

Open circuit voltage (OCV) and the voltages at two current densities (0.5 and 1 A cm^{-2}) in each freeze/thaw cycle are listed in Fig. 2. The OCV does not change, with the constant values of 1.015 V for MEA2 and 1.019 V for MEA3, respectively. The degradation rate caused by water freezing can be calculated by this method [16]:

$$\text{degradation rate (mV cycle}^{-1}) = \frac{\text{final performance (mV)} - \text{original performance (mV)}}{\text{cycle number}} \quad (1)$$

Since MEA3 was purged with a higher RH gas in the first thermal cycle, the degradation rate was calculated from the 2nd to the 20th cycle. Before freezing, the cell voltages for MEA2 are 0.7555 V at 0.5 A cm^{-2}, and 0.6539 V at 1 A cm^{-2}. After 20 cycles, the corresponding values became 0.7674 and 0.6542 V. The performance degradation rates over the whole freeze/thaw cycling range are −0.595 mV cycle^{-1} for 0.5 A cm^{-2} and −0.015 mV cycle^{-1} for 1 A cm^{-2}. For MEA3, the initial cell voltages are 0.7577 V at 0.5 A cm^{-2}, 0.6444 V at 1 A cm^{-2}. After the first cycle, the corresponding values are 0.766 and 0.6324 V. The degradation rates from the 2nd to the 20th thermal cycle are 0.226 mV cycle^{-1} for 0.5 A cm^{-2} and 0.311 mV cycle^{-1} for 1 A cm^{-2}, respectively. In each thermal cycle, the high frequency resistances of the two cells at the two current densities are also shown in Fig. 2. Taking the resistance at 0.5 A cm^{-2} for comparison, it is found to decrease from 89.2 to 84.89 mΩ cm^2 for MEA2 from the 1st to the 5th. There is only a 0.331 mΩ cycle^{-1} increase for the resistance from the 6th to the 20th. For MEA3, the cell resistance decreased from 94.9 to 93.24 mΩ cm^2 after the first cycle, and there is only a 0.136 mΩ cycle^{-1} increase within the rest of the 19 thermal cycles. The increase is very small, and three orders of magnitude of the value is caused by freeze damage [9].

Since the current density region below 200 mA cm^{-2} is typically the activation control region in an oxygen polarization curve, the voltages at 50 and 100 mA cm^{-2} are used to compare. The *IR* corrected kinetic performance of MEA2 and MEA3 in each freeze/thaw cycle is shown in Fig. 3. As expected, kinetic performance losses are not observed. The selected current densities are so low that the concentration overpotential caused by oxygen diffusion can be neglected. The interference from the hydrogen crossover is very small because the crossover is less

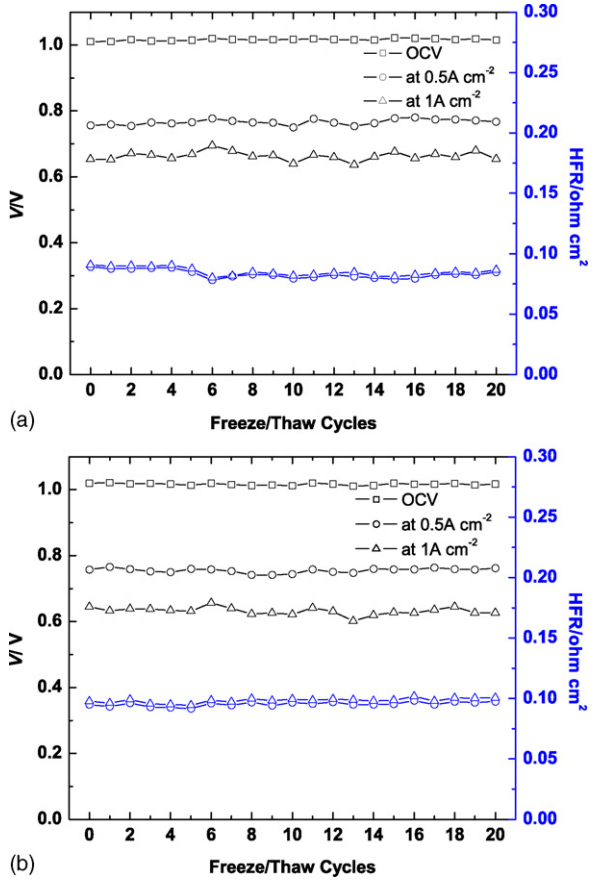

Fig. 2. The effect of the thermal cycles on performance and high frequency resistances of the two cells: (a) MEA2; (b) MEA3.

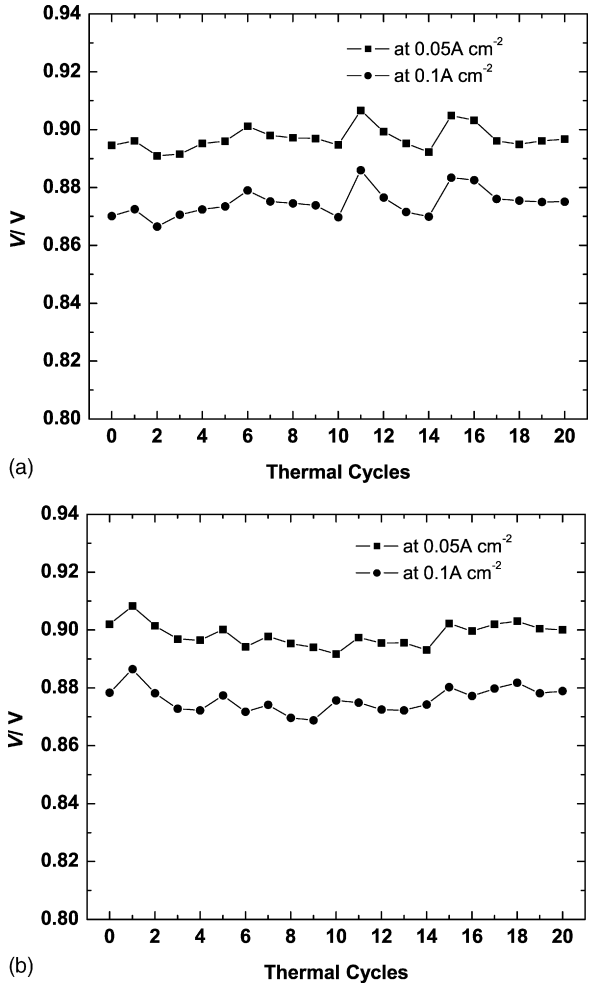

Fig. 3. IR_{HF} corrected kinetic performance of the two cells with the thermal cycles: (a) MEA2; (b) MEA3.

Table 1
The ECSAs of MEA2 and MEA3 with thermal cycles increasing

Thermal cycles	MEA2		MEA3	
	Peak area ($mC\,cm^{-2}$)	ECSA ($m^2\,g^{-1}$)	Peak area ($mC\,cm^{-2}$)	ECSA ($m^2\,g^{-1}$)
Before frozen	48.6	46.3	48.2	45.9
1st	47.8	45.4	47.8	45.4
5th	50.1	47.7	51.9	49.4
10th	52.8	50.3	46.9	44.7
15th	54.1	51.2	50.7	48.3
20th	51.1	48.7	49.3	46.9

than 1 mA cm^{-2} from our measurements. Thus, the fluctuation is due to the electrochemical active surface area of the cathode and the catalyst activity per unit mass. Since only a 20% Pt/C catalyst was applied in all experiments, the catalyst activity per unit mass must be the same. As a result, the fluctuation can be ascribed to the fluctuations in the ECSA as shown in Table 1.

3.2. Electrochemical active surface area

In addition to the polarization performance, a diagnostic test of the CV measurement was carried out to get the ECSA of Pt catalysts. The ECSA is the relation to the charge area under H-desorption peak in the CV curve, the charge area of the H-desorption on the smooth Pt and the catalyst loading in the catalyst layer. The ECSA can be calculated with following equation [20]:

$$\text{ECSA}\,(m^2\,g^{-1}) = \frac{\text{Charge area}\,(\mu C\,cm^{-2})}{10 \times 210\,(\mu C\,cm^{-2}) \times \text{Catalyst loading}\,(mg\,cm^{-2})} \quad (2)$$

The charge areas under the H-desorption peak of the MEA2 and MEA3 are integrated and listed in Table 1. In these measurements, the pressures of N_2 and H_2 at the working and counter electrodes were both 0.1 MPa. Supposing that the charge area of the H-desorption on the smooth Pt is also 210 $\mu C\,cm^{-2}$ under this condition, the ECSAs of MEA2 and MEA3 from Eq. (1) are summarized in Table 1.

From Table 1, the values of the ECSA change between 45.4 and 51.2 $m^2\,g^{-1}$ for MEA2, 44.7 and 49.4 $m^2\,g^{-1}$ for MEA3, without obvious decay. There is typically a 10% uncertainty in the CV measurements, and the ECSAs of the two cells with error bars are shown in Fig. 4. Although the ECSA of MEA3 decreases from 45.9 to 45.4 $m^2\,g^{-1}$ after the first freeze/thaw cycle, it does not decrease progressively thereafter. The linear fitting results in Fig. 4 suggest that with two different RH gases purgings, the amount of the water in the catalyst layers has been reduced to an extent (<RH 17% at 50 °C) that the destruction from ice formation was avoided. Cho et al. [21] came to the same conclusion that the ECSA fluctuated between 38.1 and 42.5 $m^2\,g^{-1}$ during seven freeze/thaw cycles with dry N_2 purging.

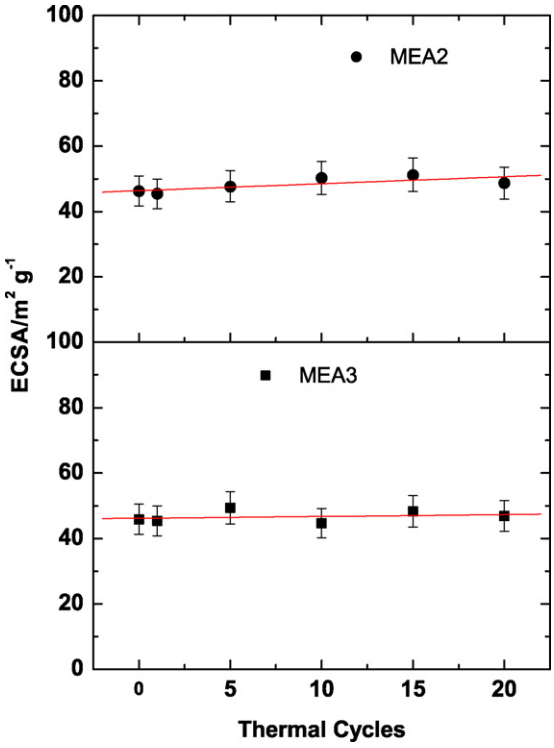

Fig. 4. The ECSAs of MEA2 and MEA3 with thermal cycles.

3.3. EIS

The dynamic EIS response of a fuel cell can provide the information about interfacial kinetics, electrode transport process, and membrane hydration. [22,23]. We measured the electrochemical impedances of the two cells operating at 0.5 and 1 A cm^{-2}.

The thermal cycle effects on the EIS responses of MEA2 and MEA3 are shown in Figs. 5 and 6. Generally, the anodic polarization is very small and can be neglected. Thus, the obtained impedance spectrum mainly reflects the cathode. The impedance spectrum includes a highest frequency intercept with the real axis, a higher frequency arc and a lower frequency arc. The highest frequency intercept denotes the sum of interfacial contact and material bulk resistance (R_1). The higher frequency arc reflects the combination of a charge transfer resistance (R_{ct}) and a double layer capacitance (C_{dl}) within the catalyst layer. The lower frequency arc reflects the mass transport process. The equivalent circuits [24] shown in Fig. 7 are applied to fit the impedance curves. Since the lower frequency arc does not appear in the impedance spectra of the two cells at 0.5 A cm^{-2}, the equivalent circuit consists of R_{ct} connected with C_{dl} in parallel and R_1 added in series. This is shown as Fig. 7a. As the impedance spectra at 1 A cm^{-2} have second arcs, a Nernst diffusion impedance in the equivalent circuit is added, as shown in Fig. 7b. The double layer capacitance is considered to be a constant phase element (CPE). Only the R_1 and R_{ct} fitting data are listed in Table 2. For MEA2, R_1 fluctuates from 79.05 to 88.89 m$\Omega\,cm^2$ at 0.5 A cm^{-2}, and from 79.55 to 87.99 m$\Omega\,cm^2$ at 1 A cm^{-2}. The value does not increase with the thermal cycles. This indicates that the sum of the membrane resistance and the contact resistance between

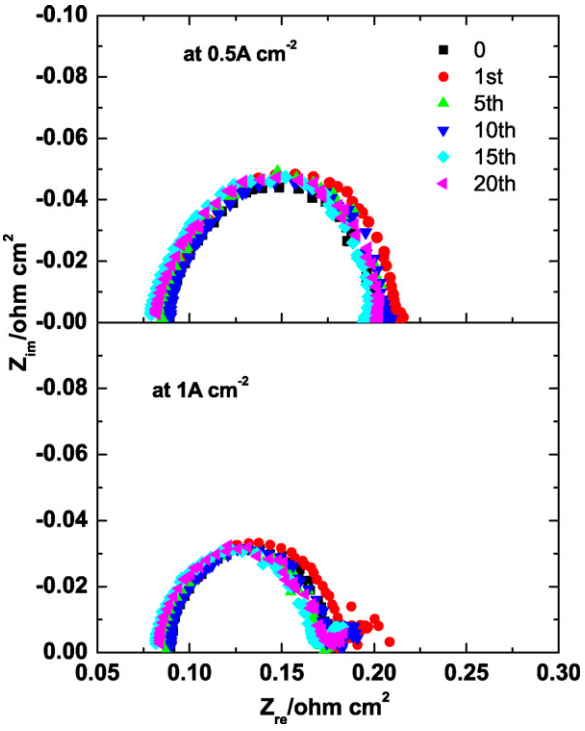

Fig. 5. The effect of the thermal cycles on the EIS responses of MEA2.

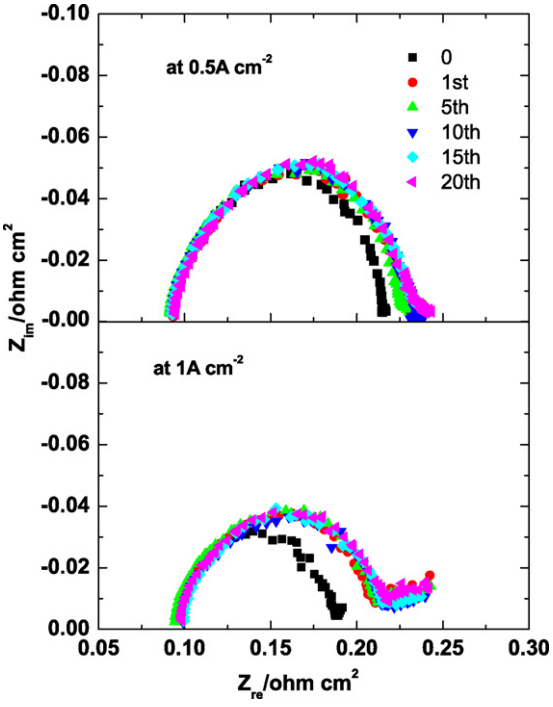

Fig. 6. The effect of the thermal cycles on the EIS responses of MEA3.

the membrane, electrodes, and bipolar plates keeps constant. In addition, from these unchanged values, it can be concluded that the membrane and electrolyte at this RH cannot be destroyed by ice formation with respect to the conductivity. The values of R_{ct} at 1 A cm^{-2} are much lower than those at 0.5 A cm^{-2} because of the faster interfacial oxygen reduction rate at higher current density. Thus, such an increasing rate results in a lower frequency arc at 3 Hz in Fig. 5. Although some mathematical models [22,23] foretold that there was no second arc in the Nyquist plot with a Nafion®112 membrane and pure O_2, the lower arc relating to the oxygen transport limitation was found in our experiments. The reason is likely that since the EIS measurements are carried out after a series of tests, more water generated increases the O_2 mass transport resistance. But it is the EIS difference between "before freeze" and "after freeze" conditions that should be noticed. From this point of view, the degradation caused by water freezing in MEA2 has been avoided. It is worth noting that RH 58.0% gas instead of dry gas purging successfully avoids electrolyte dehydration.

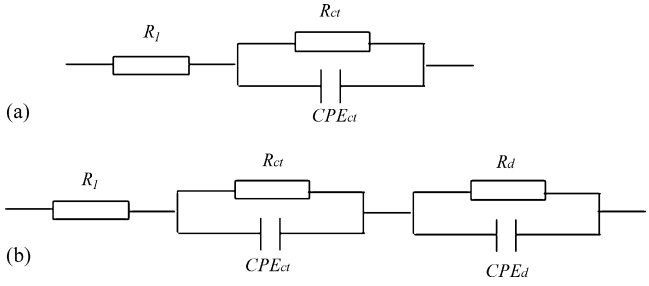

Fig. 7. The equivalent circuits: (a) without a second arc; (b) with a second arc.

Fig. 6 shows the Nyquist plots of MEA3 with freeze/thaw cycles increasing. The fitting data of R_1 and R_{ct} are also summarized in Table 2. R_1 either at 0.5 or at 1 A cm^{-2} shows no evident change. This indicates that the interface at the catalyst sides and the electrolyte proton conductivity are not negatively influenced in all cycles. From Table 2, the values of R_{ct} at the

Table 2
The fitting data for R_1 and R_{ct} of MEA2 and MEA3

Thermal cycles	MEA2 (mΩ cm^2)				MEA3 (mΩ cm^2)			
	At 0.5 A cm^{-2}		At 1 A cm^{-2}		At 0.5 A cm^{-2}		At 1 A cm^{-2}	
	R_1	R_{ct}	R_1	R_{ct}	R_1	R_{ct}	R_1	R_{ct}
0	88.57	112.9	87.99	90.58	92.79	125.1	93.95	95.16
1	87.63	125.6	86.60	98.27	92.05	138.00	93.68	120.60
5	85.44	118.6	86.17	87.83	89.92	139.6	91.46	126.10
10	88.89	118.0	87.88	88.14	91.80	132.9	95.49	124.90
15	79.05	118.6	79.55	89.10	90.92	144.5	96.24	123.90
20	81.69	122.1	81.43	91.87	92.21	145.0	95.88	124.40

two current densities increase after the first freeze. Performance loss in the activation control region was not found after the first freeze, and the ECSA of MEA3 by CV measurement shows no change over 20 freeze/thaw cycles. As a result, the R_{ct} increase ascribed to the catalyst specific surface area decrease should be considered. As we know, the charge transfer process relating to the oxygen reduction reaction (ORR) shown as formula (3) is influenced by oxygen infiltration and proton transport to the catalyst sides. Since the galvanostatic mode was adopted in the EIS measurements, the number of protons electro-migrated to the catalyst sides must be the same, and the proton electro-osmosis in the hydrated membrane must not be the limiting step. After the first freeze, the cell became easily flooded. Thus, the charge transfer process is indirectly affected by the oxygen diffusion within the diffusion layer. With current density increasing, this effect becomes more evident because of more water generated. From Table 2, R_{ct} increases from 125.1 to 138.00 mΩ cm^2 at 0.5 A cm^{-2} and from 95.16 to 120.60 mΩ cm^2 at 1 A cm^{-2} after the first freeze. Furthermore, with RH 45.0% reactant gas purging, R_{ct} does not change over all the rest thermal cycles.

$$O_2 + 4H^+ + 4e^- \rightarrow 2H_2O \quad (3)$$

3.4. Morphology and microstructure

To investigate the morphology change of the MEAs, the cross-sections of fresh MEA, MEA2, MEA3 and delaminated MEA are compared in Fig. 8. The smooth component in the middle of the pictures is the membrane and the left part is the cathode. From Fig. 8a, either cathode or anode contacts the membrane intimately. The cross-section of MEA2 in Fig. 8b is similar to the fresh one. As discussed in Sections 3.1 and 3.3, although by 58.0% reactant gas purging, the cell was frozen at −20 °C with RH 16.6% at 50 °C in it, the MEA delamination did not occur. The delaminated one is shown in Fig. 8d. Comparing Fig. 8c with Fig. 8d, it is easy to find that the interfaces of MEA3 are not influenced.

A mercury intrusion porosimetry measurement was carried out to obtain the pore size distribution in the MEAs. The pore size distribution of the fresh MEA is shown in Fig. 9. Although the pore sizes are different, only three ranges: macropores, mesopores and micropores in the GDL are paid much attention [25]. Here, the "macropores", "mesopores" and "micropores" are defined as the pore size range of 10–70, 1–10 and 0.05–1 μm, respectively. This kind of classification is based on the porosimetry data and can be carefully distinguished in Fig. 9. Here, the

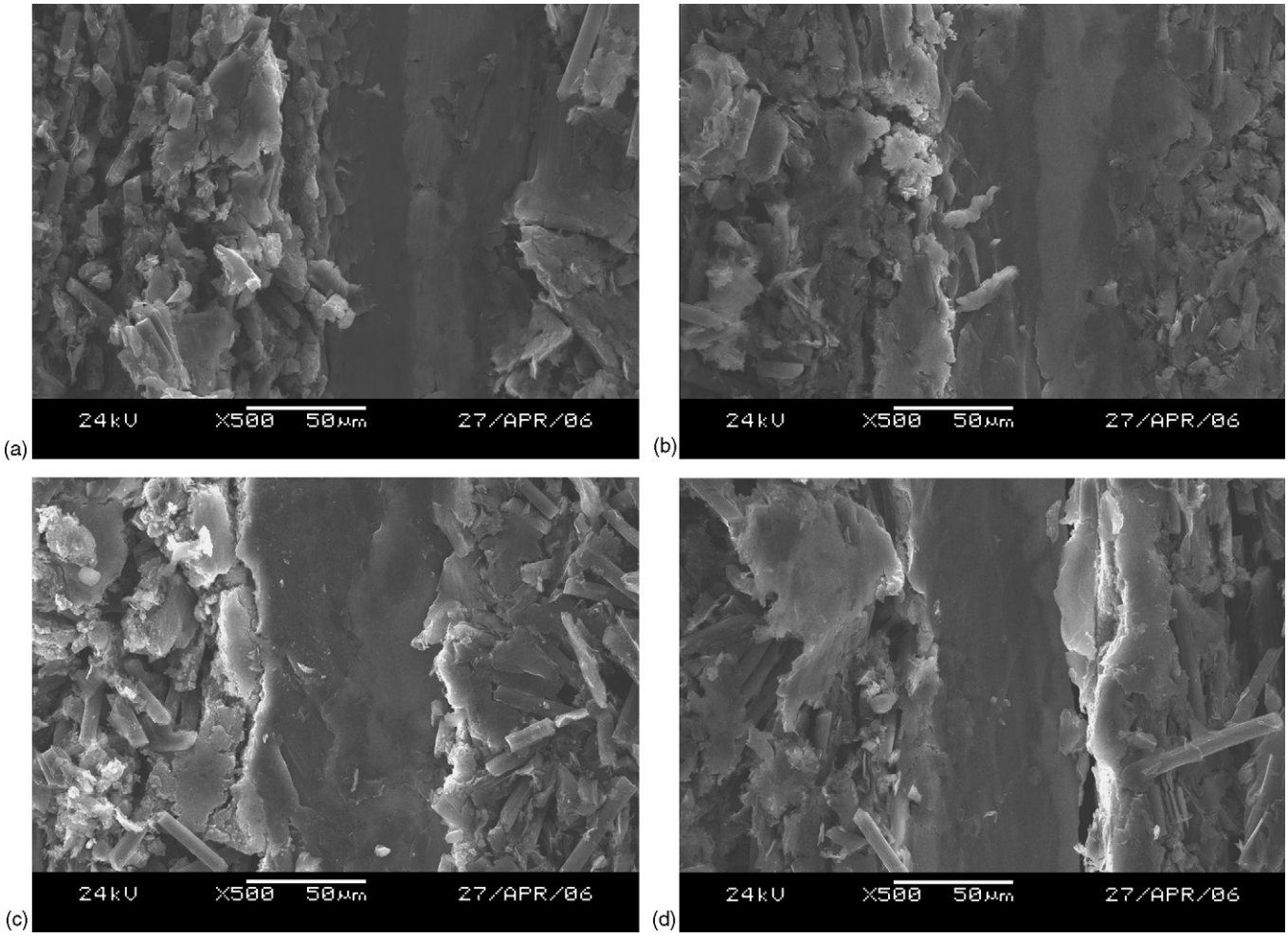

Fig. 8. SEM photographs of MEAs cross-sections: (a) fresh; (b) MEA2; (c) MEA3; (d) delaminated MEA.

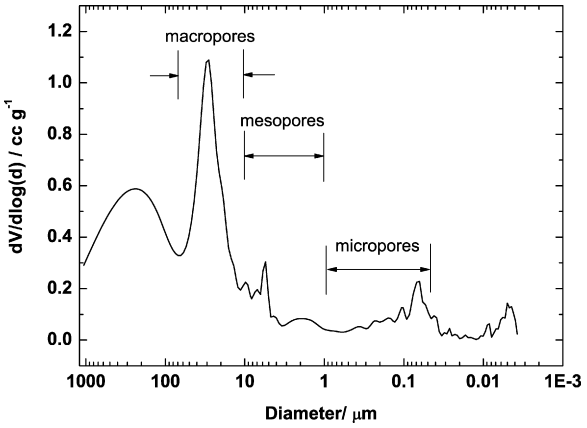

Fig. 9. Pore size distribution of the fresh MEA.

Table 3
Pore size distribution of different MEAs

Samples	Local porosity (%) in corresponding pore diameter ranges (μm)				Total porosity (%)
	0.0036–0.05	0.05–1	1–10	10–70	
Fresh	3.99	8.40	9.46	34.15	56.00
MEA2	6.41	8.21	7.84	36.21	58.67
MEA3	5.15	11.03	10.21	39.61	66.00

definition such as "macropores" is different from the general criteria and can change with the different kinds of porous materials. For comparison, we list the pore size distribution of the fresh MEA, MEA2 and MEA3 in Table 3. The macropores, mesopores and micropores porosities of the fresh MEA and MEA2 are approximately the same. These results indicate that the pore structure of MEA2 is not destroyed by water freezing at −20 °C. The porosities of MEA3 are all slightly higher than those of the fresh MEA, though the gas with a lower RH was used in the 19 freeze/thaw cycles. Therefore, the porosities of MEA3 have changed in the first few freeze/thaw cycles. The porosities of MEA2 and MEA3 in the pore size range of 0.0036–0.05 μm are all slightly higher than that of the fresh one. The whole MEA including membrane was measured and the pore size in the range is so small that it involves the membrane pore size.

4. Conclusions

The freeze degradation of PEMFC with different RHs in it was investigated through 20 freeze/thaw cycles from −20 °C to 60 °C. By continually feeding reactant gas with a RH of 58.0% at 25 °C immediately after the cell operation, MEA2 was purged to RH 16.6% at 50 °C in all 20 freeze/thaw cycles. MEA3 was purged by RH 64.9% gas in the first cycle, and then was purged to RH 12.9% by reactant gas RH 45.0% in the remaining 19 freeze/thaw cycles. After 20 freeze/thaw cycles, MEA2 was found to have no performance degradation. From the cell resistances and the EIS, the electrolyte conductivity and interfacial charge transfer resistances were constant. The ECSA from the CV measurements showed that the water amount in the CL was reduced to an extent and the destruction caused by ice formation was avoided. Although MEA3 became easily flooded at high current density after the first cycle, no further performance loss was found. The pore size distribution data indicated that the gas diffusion layer of MEA3 changed in the first freezing cycle. The SEM pictures further verified no MEA delamination. So purging with a reactant gas with a certain RH provides a feasible solution for PEMFC storage at subzero temperatures.

Acknowledgements

This work was financially supported by the National High Technology Research and Development Program of China (863 Program no. 2005AA501660) and the National Natural Science Foundation of China (no. 20206030). We also would like to thank Kikusui Electronics Corp.

References

[1] E.A. Ticianelli, C.R. Derouin, S. Srinivasan, J. Electroanal. Chem. 251 (1988) 275.
[2] M.S. Wilson, S. Gottesfeld, J. Appl. Electrochem. 22 (1992) 1.
[3] M.S. Wilson, S. Gottesfeld, J. Electrochem. Soc. 139 (2) (1992) L28–L30.
[4] M. Wakizoe, O.A. Velev, S. Srinivasan, Electrochim. Acta 40 (3) (1995) 335.
[5] M.S. Wilson, J.A. Valerio, S. Gottesfeld, Electrochim. Acta 40 (3) (1995) 355.
[6] V.A. Paganin, C.L.F. Oliveira, E.A. Ticianelli, et al., Electrochim. Acta 43 (24) (1998) 3761.
[7] S. Mukerjee, S. Srinivasan, A.J. Appleby, Electrochim. Acta 38 (12) (1993) 1661.
[8] R.C. McDonald, C.K. Mittelsteadt, E.L. Thompson, Fuel Cells 3 (2004) 208.
[9] E.A. Cho, J.J. Ko, H.Y. Ha, et al., J. Electrochem. Soc. 150 (2003) A1667.
[10] Y.S. Kim, L. Dong, M.A. Hickner, et al., Macromolecules 36 (17) (2003) 6281.
[11] M. Saito, K. Hayamizu, T. Okada, J. Phys. Chem. B 109 (2005) 3112.
[12] M. Oszcipok, D. Riemann, U. Kronenwett, et al., J. Power Sources 145 (2005) 407.
[13] J. Hayashi, K. Norinaga, N. Kudo, T. Chiba, Energy Fuels 15 (2001) 903.
[14] M. Sliwinska-Bartkowiak, G. Dudziak, R. Sikorski, et al., Phys. Chem. Chem. Phys. 3 (2001) 1179.
[15] Z. Lin, B. Yi, K. Bi, et al., CN. Patent 99, 1, 211005 (1999).
[16] J. St-Pierre, J. Roberts, K. Colbow, et al., J. New Mater. Electrochem. Sys. 8 (2005) 163.
[17] T.E. Spriger, T.A. Zawodzinski, M.S. Wilson, S. Gottesfeld, J. Electrochem. Soc. 138 (1991) 2334.
[18] T.A. Zawodzinski, C. Derouin, S. Radzinski, et al., J. Electrochem. Soc. 140 (1993) 1041.
[19] M.S. Wilson, J.A. Valerio, S. Gottesfeld, Electrochim. Acta 40 (3) (1995) 355.
[20] T.R. Ralph, G.A. Hards, J.E. Keating, et al., J. Electrochem. Soc. 144 (1997) 3845.
[21] E.A. Cho, J.J. Ko, H.Y. Ha, et al., J. Electrochem. Soc. 151 (2004) A661.
[22] T.E. Spriger, T.A. Zawodzinski, M.S. Wilson, S. Gottesfeld, J. Electrochem. Soc. 143 (1996) 587.
[23] V.A. Paganin, C.L.F. Oliveira, E.A. Ticianelli, et al., Electrochim. Acta 43 (24) (1998) 3761.
[24] M. Ciureanu, R. Roberge, J. Phys. Chem. B 105 (2001) 3531.
[25] C.S. Kong, D.-Y Kim, H.-K Lee, et al., J. Power Sources 108 (2002) 185.